Characterization of hardened cylindrical C1018 steel rods (0.14%–0.2% C, 0.6%–0.9% Mn) using photothermal radiometry

Chinhua Wang
Institute of Modern Optical Technologies, Suzhou University, Suzhou, Jiangsu, 215006, People's Republic of China and Key Lab of Modern Optical Technologies of Jiangsu Province, Suzhou, Jiangsu, 215006, People's Republic of China

Andreas Mandelis
Center for Advanced Diffusion-Wave Technologies, Department of Mechanical and Industrial Engineering, University of Toronto, Toronto, Ontario, M5S 3G8, Canada

(Received 10 February 2007; accepted 8 April 2007; published online 9 May 2007)

Frequency-domain photothermal radiometry has been used for the evaluation of the hardened case depth and the measurement of the thermophysical properties (thermal conductivity and diffusivity) of cylindrical C1018 heat-treated steel rods. The measurement results of several steel cylinders nominally hardened identically during a common heat-treating process were consistent with each other and also with mechanical indentation hardness test results. The application of the two-layer composite cylinder thermal-wave theory yielded an effective case depth within the discrete two-layer thermal-wave approximation. This technique provides a relatively simple noncontact and nondestructive method for evaluating the thermophysical parameters of layered cylindrical samples. The good fit of the experimental frequency scans to the two-layer thermal-wave model was shown to constitute a reasonable method for calibrating actual continuously decreasing hardness depth profiles by means of abrupt two-layer-equivalent profiles. © *2007 American Institute of Physics.*
[DOI: 10.1063/1.2736409]

I. INTRODUCTION

Since its emergence in the early 1980s, photothermal radiometry (PTR) has become a very powerful tool for the thermophysical characterization and the nondestructive evaluation of broad classes of materials,[1–6] including homogeneous materials[7] and layered and/or buried structures.[8] However, most studies using PTR so far have been mainly focused on flat-surface samples, for which either one-dimensional (1D) or three-dimensional theoretical models have been developed and applied in various material studies, depending on the relative size of the incident laser-beam spot size and the thermal diffusion length within the modulation frequency range of interest. Very recently, PTR was extended to the study of homogeneous cylindrical materials, in which a theoretical model was developed and experimental validation was performed[9] on steel rod samples. The PTR technique was further developed for the study of inhomogeneous (layered) cylindrical structures,[10] in which the theoretical model was validated using a stainless-steel hollow tube for simplicity, because the inner layer was air. Nevertheless, the study of cylindrical composite structures is extremely useful for the characterization and nondestructive evaluation of a wide range of industrial structures, such as cylinders with coatings and/or case hardened steels (e.g., screws and nails), to name a few. In this article, we demonstrate the application of PTR to the thermophysical characterization of case hardened C1018 cylindrical steel rods. A set of cylindrical C1018 steel samples with various diameters (D=2, 4, 6, and 20 mm) was grouped in an industrial furnace and heat treated (carburized) at the same nominal case depth of 0.04 in.. These samples were subsequently characterized with the PTR amplitude and phase based on our composite cylindrical model.[10] The effective case depths of samples with different diameters were obtained using an appropriate algorithm. The deviation of the thermophysical properties of the hardened layer from those of the unhardened core material was also obtained. All the results are in agreement with the conventional indenter hardness test results performed destructively on one of the samples from the same batch.

II. THEORETICAL MODEL

The detailed theoretical thermal-wave treatment of a two-layer cylindrical solid was described in detail in Ref. 10. The theoretical model is suitable for the characterization of an infinitely long two-layer composite cylindrical sample with arbitrary exciting laser-beam size. Figure 1 shows the illumination scheme and the cross-sectional geometry of a composite cylindrical sample consisting of two concentric regions of radii a (region I) and b (region II). The thermal-wave field of the cylindrical sample at any point can be derived based on the Green's function method. The thermal conductivity and diffusivity of regions I and II are denoted with (k_1, α_1) and (k_2, α_2), respectively. The composite cylindrical solid is externally excited by a uniform-intensity laser beam of infinite extent in the direction perpendicular to the plane of the paper in Fig. 1, which represents a transverse cross section of the infinitely long solid. The beam is assumed to be perfectly collimated along the axial direction and subtending a sector of angle θ_0. Due to the nature of the radiometric signal (Planck radiation) from opaque solids

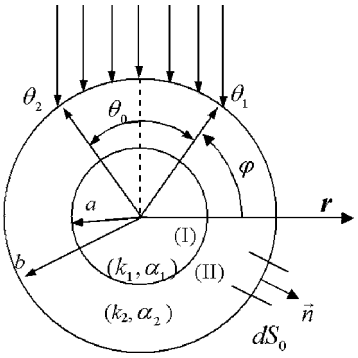

FIG. 1. Cross section of an infinitely long composite cylinder consisting of two concentric regions of radii a (region I) and b (region II) under external illumination by a uniform light beam impinging on part of its surface subtending a sector of angle θ_0.

such as metals and coatings, only the oscillating temperature of the external surface of the cylinder is of interest. The governing thermal-wave equation for region II can be written as

$$\nabla^2 T(\mathbf{r},\omega) - \sigma_2^2(\omega) T(\mathbf{r},\omega) = -\frac{1}{k_2} Q(\mathbf{r},\omega), \tag{1}$$

where $\sigma_2(\omega)=(i\omega/\alpha_2)^{1/2}=(1+i)\sqrt{\omega/2\alpha_2}$ is the thermal wave number in region II, ω is the angular modulation frequency, and $Q(\mathbf{r},\omega)$ is the volume thermal source at coordinates (r,φ) in region II of the material. Equation (1) can be solved in curvilinear coordinates by the Green's function method based on appropriate boundary conditions (Ref. 11, Chap. 6, p. 413). In the case of metallic opaque materials, which is the major focus in this article, optical absorption of a laser beam by the sample leads to thermal energy conversion essentially at the surface. The thermal coupling (loss) coefficient between a metallic solid and the surrounding gas (air) is on the order of 10^{-3}.[9] Therefore, the adiabatic second kind (Neumann) boundary condition at the external surface can be applied, and the volume thermal source $Q(\mathbf{r}_0,\omega)$ can be neglected. The boundary conditions for the temperature field can be written as

$$k_2 \frac{\partial}{\partial n} T(\mathbf{r}_0,\omega)\bigg|_{r_0=a} = h_1 T(|\mathbf{r}_0;\omega)|_{r_0=a}, \tag{2a}$$

$$k_2 \frac{\partial}{\partial n} T(\mathbf{r}_0,\omega)\bigg|_{r_0=b} = F_2(\mathbf{r}_0,\omega)|_{r_0=b}, \tag{2b}$$

where h_1 (W m^{-2} K^{-1}) is the heat transfer coefficient at the inner surface S_1. F_2 is the heat flux (W m^{-2}) imposed on the exterior surface, which can be expressed as

$$F_2(b,\varphi_0;\omega) = \begin{cases} F_0 \cos(90^\circ - \varphi_0), & \theta_1 \leqslant \varphi_0 \leqslant \theta_2 \\ 0 & \text{other angles,} \end{cases} \tag{3}$$

where a projection factor in the form of the cosine of the incident uniform light intensity on the exterior surface is considered. Therefore, in the absence of volume thermal sources in region II and in the underlying region I, the general thermal-wave field can be represented by

$$T(r,\varphi,\omega) = \frac{\alpha_2 F_0 b}{k_2} \oint_{S_2} G(\mathbf{r}|\mathbf{r}_0;\psi)\cos(90^\circ - \varphi_0) d\varphi_0. \tag{4}$$

In Eq. (2a) the third kind of boundary condition represents the most general type of boundary condition which can be reduced to the temperature continuity at $r=a$ when $h_1=0$. The solution can be obtained as per our earlier treatment of a hollow cylinder;[10] however, in the present case where intimate coupling between the two solid regimes I and II exists at $r=a$, h_1 will be replaced by the thermal parameters of the inner material using the formal equivalence between a hollow cylinder and a two-layer solid cylinder (Ref. 11, Chap. 5.24, p. 388).

The appropriate Green's function $G(\mathbf{r}|\mathbf{r}_0;\omega)$ to be used in Eq. (4) can be written with the observation coordinate, r, as the running variable in the form[10]

$$G(\mathbf{r}|\mathbf{r}_0;\omega) = \frac{1}{2\pi\alpha_2} \sum_{m=-\infty}^{\infty} \frac{e^{im(\varphi-\varphi_0)}}{[Y_m(b) - X_m(a)]} \times \begin{cases} K_m(\sigma_2 r_0)[K_m(\sigma_2 r) - X_m(a) I_m(\sigma_2 r)] - Y_m(b) I_m(\sigma_2 r_0)[K_m(\sigma_2 r) - X_m(a) I_m(\sigma_2 r)] & (a \leqslant r \leqslant r_0) \\ K_m(\sigma_2 r)[K_m(\sigma_2 r_0) - X_m(a) I_m(\sigma_2 r_0)] - Y_m(b) I_m(\sigma_2 r)[K_m(\sigma_2 r_0) - X_m(a) I_m(\sigma_2 r_0)] & (r_0 \leqslant r \leqslant b) \end{cases} \tag{5}$$

where $I_m(z)$ and $K_m(z)$ are the complex-argument modified Bessel functions of the first kind and of the second kind of order m, respectively, and

$$X_m(a) \equiv \frac{K_m'(\sigma_2 a) - \eta_{1m} K_m(\sigma_2 a)}{I_m'(\sigma_2 a) - \eta_{1m} I_m(\sigma_2 a)} \quad (m = 0,1,2,\ldots), \tag{6}$$

$$Y_m(b) \equiv \frac{K_m'(\sigma_2 b)}{I_m'(\sigma_2 b)} \quad (m = 0,1,2\ldots), \tag{7}$$

$$\eta_{1m} \equiv \frac{I_m'(\sigma_1 a)}{\beta_{21} I_m(\sigma_1 a)} \quad (m = 0,1,2,\ldots), \tag{8}$$

and

$$\beta_{21} \equiv k_2/k_1. \tag{9}$$

Substituting Green's function $G(\mathbf{r}|\mathbf{r}_0;\omega)$, Eq. (5), into Eq. (3) and after some algebraic manipulation, we finally obtain the thermal-wave field in region II,

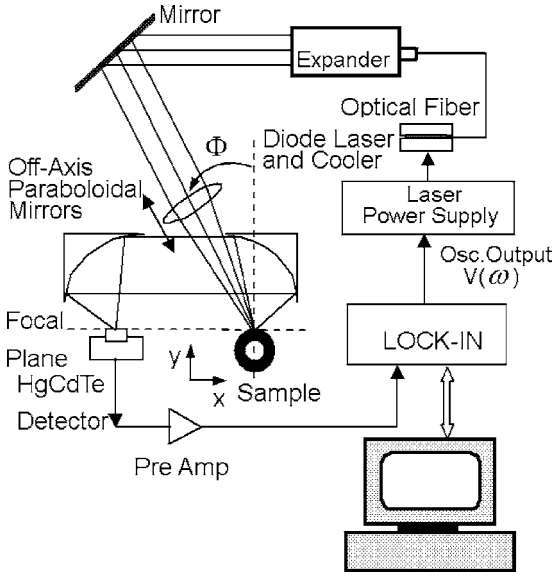

FIG. 2. Experimental setup for PTR measurement of cylindrical solids.

$$T(r,\varphi,\omega)=\frac{F_0}{2\pi k_2}\left(2\left\{\frac{K_0(\sigma_2 r)-X_0(a)I_0(\sigma_2 r)}{I_0'(\sigma_2 b)[Y_0(b)-X_0(a)]}\right\}\sin\frac{\theta_0}{2}+\left\{\frac{K_1(\sigma_2 r)-X_1(a)I_1(\sigma_2 r)}{I_1'(\sigma_2 b)[Y_1(b)-X_1(a)]}\right\}(\theta_0+\sin\theta_0)\cos\left(\frac{\pi}{2}-\varphi\right)+2\sum_{m=2}^{\infty}\left\{\frac{K_m(\sigma_2 r)-X_m(a)I_m(\sigma_2 r)}{I_m'(\sigma_2 b)[Y_m(b)-X_m(a)]}\right\}\cos\left[\frac{m}{2}(\pi-2\varphi)\right]\left\{\frac{\sin[(m+1)\theta_0/2]}{m+1}+\frac{\sin[(m-1)\theta_0/2]}{m-1}\right\}\right). \quad (10)$$

Here $X_m(a)$ and $Y_m(b)$ $(m=0,1,2\ldots)$ are given in Eqs. (6)–(9). Equation (10) gives the thermal-wave field at any point inside region II. From the structure of this expression, it is seen that the frequency dependence of the thermal-wave field of cylindrical samples under uniform illumination is a function of the thermophysical properties and geometrical dimensions of both interior and exterior materials.

III. SAMPLE DESCRIPTION AND EXPERIMENTS

The experimental setup is shown in Fig. 2. The optical excitation source was a high power semiconductor laser (Jenoptik JOLD-X-CPXL-1L ~20 W). The output of the laser was modulated by a periodic current driver (high power laser diode driver, Thor Labs), the frequency of which was controlled by the computer and also served as the lock-in amplifier reference. The beam was expanded, collimated, and then focused onto the surface of the sample with a spot size ranging from ~1 to 21 mm by adjusting the position of the converging lens. The harmonically modulated infrared radiation from the sample surface was collected by an off-axis

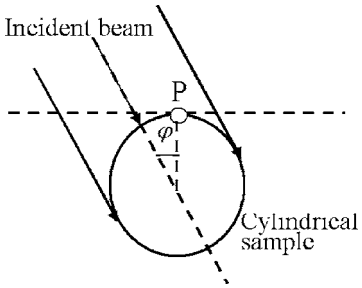

FIG. 3. Relative orientation of the incident beam and the curved sample surface.

paraboloidal mirror system and detected by a HgCdTe detector (EG&G Judson, model J15016-M204-S204-S01M-WE-60). The signal from the detector was amplified by a low-noise preamplifier (EG&G Judson PA101) and then fed into a lock-in amplifier (EG&G Instruments, model 7265) interfaced with a PC. The samples under test were a set of case hardened cylindrical C1018 steel rod with diameters ranging from 2 to 20 mm (composition: 0.14%–0.2%C, 0.6%–0.9%Mn). All the samples were hardened (carburized) together in one batch. The nominal hardening case depth was 0.04 in. The actual case depth was measured using the conventional mechanical indentation method.

The experimental setup was initially optimized using a flat sample such that both sample and detector were at the focal plane of the off-axis mirrors, as shown in Fig. 2. When the flat sample was replaced by a cylindrical surface, some adjustment had to be made such that the topmost point of the sample (i.e., the point lying on the tangent plane to the sample curvature, Fig. 2) was exactly placed (within experimental error) at the focal point of the paraboloidal mirror system. Therefore, the detector was monitoring the thermal-wave field emissions from this point. Thermal radiation information from other points of the sample would not be received by the detector, which is especially true for curved surfaces due to the strong defocusing (receding) effect of the curvature. The detailed orientation of the sample and the incident beam, as arranged in our experiment, is shown in Fig. 3. The exciting beam was incident onto the sample at angle φ. The measurement point is at angle φ (point P) if the cylinder is ideally aligned and adjusted. In the experiment, however, the measurement point could deviate from point P due to unavoidable positioning errors. Therefore, before each experiment and after positioning the sample, the angle φ must be determined. The actual measurement angle could be determined through fitting the data to the theory. After this adjustment, the laser beam was expanded to ~20 mm in diameter by moving the lens so that the beam was large enough to conform to the "infinite" z-axis illumination assumed in the model and also in order to validate the 1D model in the case of a flat sample and a flat laser-beam power profile.

Typical experimental results and the corresponding fits are shown in Figs. 4 and 5, for D=2 and 20 mm, respectively, representing the two extremes of cylindrical dimensions among our samples. The experimental amplitudes and phases in Figs. 4 and 5 are normalized to the corresponding

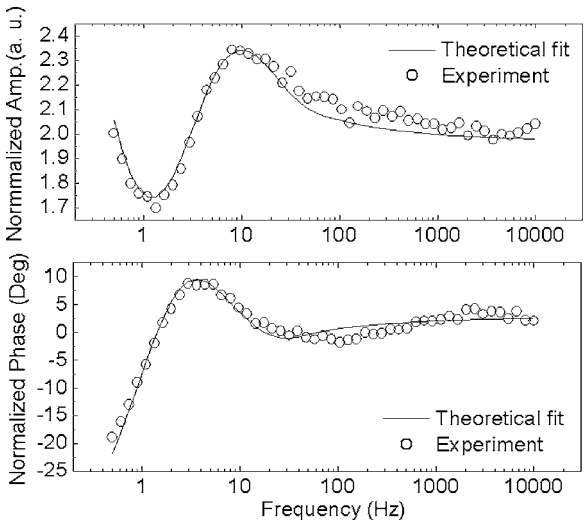

FIG. 4. Experimental results and the best theoretical fit [Eq. (10)] for a cylindrical sample with a 2 mm diameter.

signals of a flat unhardened C1018 steel sample for the purposes of (1) eliminating the instrumental function of the system and (2) eliminating the large base line in both amplitude and phase and hence enhancing the features of the curved surface. Four parameters were set as the fitting parameters. They are thermal conductivity and thermal diffusivity of the hardened layer (k_2, α_2), the effective thickness of the hardened layer L_1, and the measurement angle φ. The parameters of the unhardened core part (C1018 steel) of the cylindrical sample are assumed to be[15] $k_1=51.9$ W/m K and $\alpha_1=13.57\times10^{-6}$ m^2/s. The best-fit procedure was performed using the experimental phase data in Figs. 4 and 5 and the theoretical formula [Eq. (10)]. The corresponding theoretical amplitude values were calculated using the phase-fitted parameters and were fitted to the experimental amplitudes. The best-fitted results are shown in Table I. It was found that all the results are reasonably consistent considering the poorly controllable heat-treating process, which usually shows a

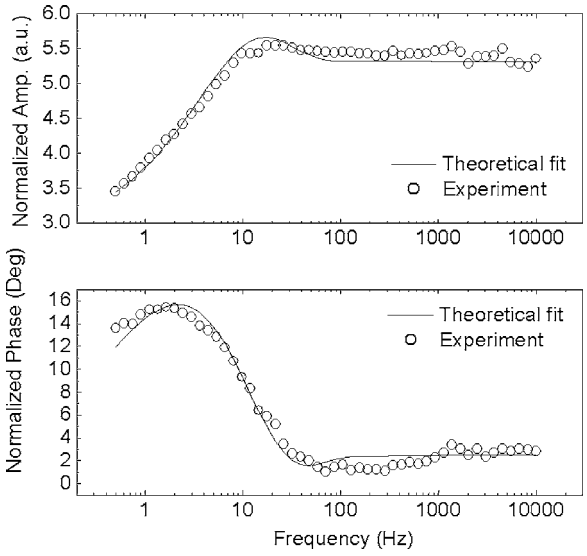

FIG. 5. Experimental results and the best theoretical fit [Eq. (10)] for a cylindrical sample with a 20 mm diameter.

TABLE I. Fitting results of hardened cylindrical samples with different diameters.

Diameter (mm)	Fitted thermal conductivity (W/m K)	Fitted thermal diffusivity ($\times10^{-6}$ m^2/s)	Fitted case depth (μm)	Fitted measurement angle φ (deg)
2.0	20.2	9.0	589.7	85.4
4.0	22.9	8.3	476.2	53.5
6.0	17.1	8.7	480.9	48.0
20.0	19.8	10.5	516.7	45.1

10%–20% fluctuation in hardness for samples from the same batch.[12] The effective case depths of the four samples lie in the range of ~500 μm, with a fluctuation of ~20%. To verify the results of the fitted case depth, one sample from the same batch of cylindrical samples was chosen to undergo mechanical indentation testing. The test was performed at three different locations of the sample, and the results are shown in Fig. 6. It is seen that the total subsurface extent of the hardened layer is ~1000 μm. Arbitrarily defining the effective case depth as the depth where the hardness decreases down to half its maximum hardness, the effective case depths from the three curves in Fig. 6 are 655, 595, and 581 μm, respectively. Our best-fitted case depth lies at approximately the middle of the total depth and is very close to the accepted effective case depth of the mechanical hardness test. It is seen that there is a systematic deviation (~100 μm) between the best-fitted case depth (shorter) and the mechanical test results which may be easily calibrated using a definition of the case depth consistent between mechanical and photothermal depth profiles. In Figs. 4 and 5 it is noted that there exist some discrepancies between the theoretical fits and the experiments, especially in the middle frequency range around 50–100 Hz, equivalent to thermal diffusion lengths of ~300–212 μm. This can be explained by the fact that the thermophysical properties in the hardened layer are not constant, and there is also no physical boundary between the hardened layer and the unhardened core part but rather a gradual change of hardness, as illustrated in Fig. 6. Because the hardness depth profile is an inhomogeneous layer with continuously varying thermophysical parameters from the surface to the unhardened core part of the cylindrical sample, the method developed in this article is only approximately valid since it uses a two-distinct-layer equiva-

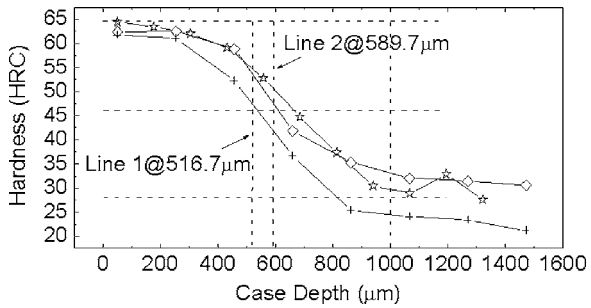

FIG. 6. Results of mechanical indentation hardness measurement for a sample with nominal 0.04 in. case hardening. For statistical purposes tests were performed at three different locations on the sample.

lence in which an "abrupt" boundary between the hardened layer and the unhardened core part is assumed. This complication causes poorer than ideal confinement of the thermal wave in the upper layer and results in less pronounced standing wave extrema than the theoretical expectations. Nevertheless, the important thermophysical parameter values can be accurately extracted from fitting the entire experimental frequency scan to the corresponding theoretical model, thus validating the use of the two-layer theory with continuously inhomogeneous case hardened steels. The effective case depths derived in Table I are consistently short compared to the full extent of the continuously inhomogeneous hardness layer. This is understandable since decreasing hardness amounts to increasing thermal diffusivity[13] which, in turn, would yield a longer thermal diffusion length if the diffusivity gradient was accounted for properly as it has been done with noncurvilinear solids.[14] An important feature of the present approximation with regard to depth profilometry of hardened steels is the conclusion that the relative goodness of the theoretical two-layer fit to the experimental frequency scans, as demonstrated by the constancy of the effective case depth (Table I), can be used to (a) calibrate the method using a step-function equivalence between two discrete layers and actual industrially heat-treated steels with continuously varying hardness profiles, provided that the latter are measured independently, or (b) offer a concrete and fast nondestructive methodology for determining effective case depths for use in developing industrial hardness depth charts under specific heat-treating processes, without the need to perform time-consuming destructive indenter analyses of the full depth profile. The development of a theoretical thermal-wave model with depth-dependent thermophysical properties in curvilinear coordinates is a challenge currently under investigation by our group.

In summary, the feasibility of measuring the hardened case depth and the thermophysical properties (thermal conductivity and diffusivity) of cylindrical C1018 heat-treated steel rods has been demonstrated. By using a cylindrical two-layer model and a multiparameter fitting algorithm, the *effective* case depth and the corresponding thermal conductivity and thermal diffusivity of the hardened layer are obtained for a nominal 0.04 in. case depth hardening. The measurement results from various samples in the same batch of heat-treated cylinders are consistent with each other and also consistent with the mechanical indentation hardness test results in the sense of yielding an effective case depth within the discrete two-layer thermal-wave approximation. This technique provides a noncontact and nondestructive method for evaluating the thermophysical parameters of layered cylindrical samples by best fitting the theoretical model to the experimental data over the entire frequency range of interest. The good fit of the experimental frequency scans to the two-discrete-layer thermal-wave model further yields a simple method for calibrating actual continuously decreasing hardness depth profiles by means of abrupt two-layer-equivalent profiles.

ACKNOWLEDGMENTS

The authors wish to acknowledge the support of the Ontario Centers of Excellence (OCE) and of Metex Heat Treating, Ltd., for this project. The support of the educational committee of Jiangsu Province (Contract No. Q2108608) and of an initializing research fund of Suzhou University (Q4108612) to one of the authors (C.W.) is gratefully acknowledged.

[1] P. E. Nordal and S. O. Kanstad, Phys. Scr. **5–6**, 659 (1979).
[2] R. D. Tom, E. P. O'Hara, and D. Benin, J. Appl. Phys. **53**, 5392 (1982).
[3] R. Santos and L. C. M. Miranda, J. Appl. Phys. **52**, 4194 (1981).
[4] L. Fabbri and P. Fenici, Rev. Sci. Instrum. **66**, 3593 (1995).
[5] T. T. Lan, H. G. Walther, G. Goch, and B. Schmitz, J. Appl. Phys. **78**, 4108 (1995).
[6] M. Munidasa, F. Funak, and A. Mandelis, J. Appl. Phys. **83**, 3495 (1998).
[7] H. K. Park, C. P. Grigoropoulos, and A. C. Tam, Int. J. Thermophys. **16**, 973 (1995).
[8] A. Salazar, A. Sanchez-Lavega, and J. M. Terron, J. Appl. Phys. **84**, 3031 (1998).
[9] C. Wang, A. Mandelis, and Y. Liu, J. Appl. Phys. **96**, 3756 (2004).
[10] C. Wang, A. Mandelis, and Y. Liu, J. Appl. Phys. **97**, 014911 (2005).
[11] A. Mandelis, *Diffusion-Wave Fields: Mathematical Methods and Green Functions* (Springer, New York, 2001).
[12] C. Wang and A. Mandelis, NDT & E Int. **40**, 158 (2007).
[13] L. Nicolaides, A. Mandelis, and C. J. Beingessner, J. Appl. Phys. **89**, 7879 (2001).
[14] A. Mandelis, F. Funak, and M. Munidasa, J. Appl. Phys. **80**, 5570 (1996).
[15] *Metals Handbook* 10th ed. (ASM International, Material Park, OH, 1990), Vol. 1, p. 196.